A quasi-3D approach for the assessment of induced AC interference on buried metallic pipelines

A quasi-3D approach for the assessment of induced AC interference on buried metallic pipelines

Arturo Popoli[a,*], Leonardo Sandrolini[a], Andrea Cristofolini[a]

[a]*Department of Electrical, Electronic and Information Engineering, University of Bologna, Bologna, 40136, Italy*

Abstract

In this paper, a novel quasi-three dimensional technique for the study of electromagnetic interferences induced by overhead power lines on buried metallic pipelines located in the same corridor is proposed. The aim of the method is to provide an inherently three dimensional solution to the problem, by using a two dimensional finite element approach. According to the proposed methodology, a bidimensional quasi-magnetostatic analysis is performed on a section of the considered corridor. The three dimensional extension is obtained by using a circuital approach to consistently couple the analysed section with the rest of the system. The analysis of the obtained equivalent circuit finally provides the actual values of the longitudinal electric fields acting on the studied section, and thus allows the solution of the problem. The results obtained from the described procedure have been compared for a few simple interference cases with those obtained using Carson's analytical formulas for the calculation of mutual impedances. Finally, a study on the effects of a non-homogeneous soil structure has been carried out.

Keywords: Electromagnetic compatibility, electromagnetic coupling, finite element analysis, pipelines, equivalent circuits.

*Corresponding author

Email address: arturo.popoli@unibo.it (Arturo Popoli)

1. Introduction

Throughout the years, a number of works dealing with this matter have been based on representing the pipeline as a lossy transmission line, with one or multiple voltage sources representing the electromotive force induced by the power line [1–3]. The majority of these works (including the approach proposed by Cigré, which is used as a meter of comparison with this work) rely on some approximation of Carson's formulae for the computation of the mutual impedance between the power line phase and overhead ground conductors and the metallic pipeline. During the course of the years many improvements have been made in the framework of these "analytical" methods, mainly regarding the accounting of multi-layered soils [4] and non-parallel geometric dispositions of the conductors [5]. The accuracy of the aforementioned methods has been experimentally tested, and proved to be good for very simple geometries [6]. However, a common feature among all these works is that the provided formulations stem from assuming a "weak coupling" hypothesis between the metallic conductors. This implies, for example, that the effects on the conductors of the power line (or other pipelines) produced by the current flowing through the pipeline are neglected. Likewise, whenever multiple OGWs are present, the mutual induction between themselves is neglected, as well as their second order interaction with the pipeline(s). Conversely, the methods based on the finite element analysis can overcome the aforementioned limitations, granting the possibility of a detailed and accurate analysis of arbitrarily complex physical domains. However, a full 3D analysis of the whole corridor would require an extremely large number of elements, yielding a considerable computational effort. Hence, a number of bidimensional methods have been developed [7, 8], relying on the assumption of a preferential (axial) direction of the power line currents. In this fashion, the work in [7] has shown how a two dimensional Finite Element Method (2D-FEM) can be used to calculate the self and mutual impedances of the conductors of a given physical configuration, which are subsequently employed for building an equivalent lumped parameters network. In work presented in this paper, the FEM analysis is not simply used to extract the

circuital parameters of a configuration. Rather, the circuit analysis is a tool used for the 2D-FEM analysis to take into account the physical constraints stemming from the inherent three dimensionality of the problem. Hence, a self-consistent methodology to couple a quasi-magnetostatic 2D-FEM analysis of a section of the given corridor with the rest of the system is developed. This is obtained by defining a multi-port electrical component which, if subjected to a given set of forcing terms, produces the same currents that would result from an FEM calculation. As a result, the quantities obtained from the circuit analysis, reintroduced in the FEM code, will produce results that are consistent with the constraints enforced by the circuit analysis itself. In this way, some of the inherently 3D features that cannot be addressed in a 2D formulation are naturally taken into account, such as the soil acting as a return path for the currents of the pipeline and the overhead ground wires (OGWs), the pipeline earthings or the leakage currents due to an imperfect pipeline coating. In other words, the network introduces the appropriate constraints on the FEM analysis to account for the aforementioned phenomena. Section 2 shows the details about how the 2D-FEM analysis is performed on a corridor section, and how the constitutive law of the aforementioned multi-port is extracted. Then, the process for the network construction and the subsequent solution is shown. In Section 3 the proposed approach is validated by means of a comparison with the approach proposed by Cigré, and some further tests are performed for various physical configurations and soil structures. It is also shown that an interpolation technique can be consistently used to extend the range of applicability of the computed results.

2. Methodology description

The proposed methodology articulates in a series of steps, described in the following subsections. The first one is the implementation of a 2D-FEM solver (Sec. 2.1), subsequently used to provide the results needed for the construction of the *characteristic* matrix $[\boldsymbol{M}]$, as described in Sec. 2.2. Finally, the information contained in $[\boldsymbol{M}]$ is employed for building an equivalent electrical circuit, to be

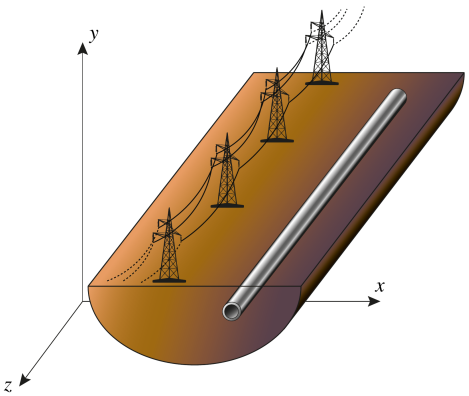

Figure 1: Representation of a power line (left) and a parallel metallic pipeline (right) buried in the soil (drawing not in scale).

solved with some kind of mesh analysis technique (Sec. 2.3).

2.1. 2D-FEM formulation

As already anticipated, the presented method's foundation is a series of 2D-FEM simulations of the geometry under analysis. The FEM code employed in the framework of this work shares the basic setting with the ones described in [9, 10]. It is based on the assumption of linearity and isotropy of the materials, infinite length of the conductors along the z axis (referring to Fig. 1) and a quasi-magnetostatic regime (i.e., the displacement current is negligible with respect to the conduction current in the conductors). For the aforementioned hypotheses, now $\vec{J} = J_z(x, y)\hat{k}$, $\vec{A} = A_z(x, y)\hat{k}$, and one can write:

$$J_z = J_{z,0} - \sigma \frac{\partial A_z}{\partial t}, \tag{1}$$

where $J_{z,0}$ represents the current density that one would find if the problem was stationary, whereas the $-\sigma\ \partial A/\partial t$ term accounts for the currents produced by the magnetic induction, through Faraday's law. The diffusion of the magnetic vector potential A_z is described by:

$$-\nabla \cdot \left(\frac{1}{\mu} \nabla A_z \right) = J_{z,0} - \sigma \frac{\partial A_z}{\partial t}, \tag{2}$$

where $\mu = \mu_0\mu_r$ and σ represent the magnetic permeability and the electrical conductivity of the given meshed physical media, respectively. If a sinusoidal steady-state regime is assumed for the line currents of the power line, (2) can be rewritten as:

$$-\nabla \cdot \left(\frac{1}{\mu}\nabla \boldsymbol{A}_z\right) = \boldsymbol{J}_{0,z} - j\omega\sigma \boldsymbol{A}_z, \tag{3}$$

where the bold notation is employed for the physical quantities described by complex phasors. The FEM involves the discretization of both the calculation domain (resulting in a triangular mesh) and (3). The latter is generally performed employing some kind of piecewise polynomial representation $\tilde{\boldsymbol{A}}_z$ of the unknown function. This is obtained defining a set of shape functions $\{N\}$ as a basis of the piecewise polynomial representation and letting $\tilde{\boldsymbol{A}}_z = \{N\}^T\{\boldsymbol{A}_z\}$, where $\{\boldsymbol{A}_z\}$ is an array whose elements are the nodal approximated values of $\boldsymbol{A}_z$. Applying the so-called *Galerkin approach*, a weak formulation [11] of the resulting weighted residuals approach can be written as:

$$\int_\Omega \nabla N_k \cdot \left(\frac{1}{\mu}\nabla \tilde{\boldsymbol{A}}_z\right) \mathrm{d}S + j\omega \int_\Omega N_k \sigma \tilde{\boldsymbol{A}}_z \mathrm{d}S = \int_\Omega N_k \boldsymbol{J}_{0,z} \mathrm{d}S - \oint_{\partial\Omega} N_k \frac{1}{\mu}\frac{\partial \tilde{\boldsymbol{A}}_z}{\partial n}\mathrm{d}l, \tag{4}$$

where Ω stands for the calculation domain, and $\partial\Omega$ for its boundary. Equation (4) can be written for each node of the mesh, thus yielding a complex linear system, here reported:

$$[\boldsymbol{K}]\{\boldsymbol{A}_z\} = \{\boldsymbol{f}\} \tag{5}$$

The finite element code used in this work implements the model described so far, utilizing a first order set of shape functions defined on a triangular mesh. A combination of structured and Delaunay triangulation can be used according to the needs. The code is written in FORTRAN 90 and is compiled using the Intel Fortran Compiler. The linear system (5) is solved by means of the Intel MKL PARDISO parallel routines [12], which compute a direct solution through the reordering and subsequent LU factorization of the coefficient matrix. A single run of the FEM solver takes about 3.31 s of CPU time on an i7-7700HQ CPU with 4 cores and 16 Gb of RAM to obtain the solution for a 66121 nodes mesh. In

(5), for a given problem geometry, the coefficient matrix $[\boldsymbol{K}]$ is a sparse complex matrix depending on the material properties (i.e., conductivities and magnetic permeability) of the materials involved, while the right hand side takes into account the imposed current densities $\boldsymbol{J}_{0,z}$ and the boundary conditions applied to $\partial\Omega$. The system in (5) represents the relationship between the forcing terms of the problem (i.e., the imposed current densities $\boldsymbol{J}_{0,z}$) and the vector potential distribution on the 2D domain under investigation. It should be noted that the forcing terms are related to the longitudinal electric fields, and are generally not known a priori, since they depend on what is upstream and downstream in the corridor. Hence, in order to solve the problem, it is necessary to provide a way to model the coupling between the section taken into consideration and the rest of the corridor. The method used to accomplish this task will be discussed in the next sections.

2.2. Characteristic matrix construction

As stated in the previous section, the system (5) resulting from the FEM procedure defines a relationship between the problem forcing terms and the effects caused by them in the considered domain. It is useful to emphasize that, thanks to the hypothesis of linear materials stated in Sec. (2.1), this relationship is linear. Thus, considering a geometry with n conductors (i.e., line conductors, OGWs, pipelines..., and the soil which is considered a conductor too), the linear relationship between the electric current flowing in each conductors and the imposed current densities can be written as follows:

$$\{\boldsymbol{I}\} = [\boldsymbol{M}]\{\boldsymbol{J}_{z,0}\}. \tag{6}$$

In (6), the arrays $\{\boldsymbol{I}\}$ and $\{\boldsymbol{J}_{z,0}\}$ contain the n electric currents $\boldsymbol{I}_1, \boldsymbol{I}_2, \ldots, \boldsymbol{I}_n$ and imposed current densities $\boldsymbol{J}_{z,0,1}, \boldsymbol{J}_{z,0,2}, \ldots, \boldsymbol{J}_{z,0,n}$ on the conductors, respectively. Equation (6) is a definition of the characteristic matrix $[\boldsymbol{M}]$, which is a a rank n complex square matrix expressing the linear relation between the arrays $\{\boldsymbol{I}\}$ and $\{\boldsymbol{J}_{z,0}\}$. The generic element $m_{h,k} \in [\boldsymbol{M}]$ is the current flowing through the hth conductor when a unit current density $\boldsymbol{J}_{0,z,k}$ is enforced on the kth one.

In order to build the characteristic matrix, n simulations have to be run (one for each meshed conductor). Considering the kth run, a unit current density $\boldsymbol{J}_{0,z,k} =$

1 A/m^2 is enforced on the kth conductor, while $\boldsymbol{J}_{0,z}$ is set to 0 for the remaining $n-1$ conductors.

The phasorial representation of the current density is obtained from (1) :

$$\boldsymbol{J}_z = \boldsymbol{J}_{0,z} - j\omega \boldsymbol{A}_z, \tag{7}$$

and the total current $\boldsymbol{I}_i$ on the generic ith conductor is computed by integrating $\boldsymbol{J}_z$ over the conductor cross section S_i:

$$\boldsymbol{I}_i = \int_{S_i} \boldsymbol{J}_z \mathrm{d}S. \tag{8}$$

Therefore, each run of the code produces n currents $\boldsymbol{I}_1, \boldsymbol{I}_2, \ldots, \boldsymbol{I}_n$, used to fill the kth column of $[\boldsymbol{M}]$. This process is schematically shown in Fig. 2. As already mentioned, the soil (or, more precisely, the part of the soil that is involved as an electrical conductor) is regarded as a standard conductor, just like all the others. Because of this, the depicted ground symbol of Fig. 2 assumes then the meaning of "distant earth", i.e., a perfect return path with $\boldsymbol{Z} = 0\ \Omega$ for all the considered currents. The characteristic matrix $[\boldsymbol{M}]$ depends only on the geometry of the physical domain and on the electrical properties of the materials. Once $[\boldsymbol{M}]$ is available for a given geometry, one may regard (6) as a relationship that is in all respects equivalent to the FEM analysis, in the sense that for a given set of forcing terms $\{\boldsymbol{J}_{z,0}\}$, (6) yields the same currents that would have been obtained from an FEM calculation. Conversely, from (6), one may obtain the forcing terms $\{\boldsymbol{J}_{z,0}\}$ that would yield a given set of currents $\{\boldsymbol{I}\}$. On the other hand, (6) may be regarded as a constitutive law of an n-port circuit element, that may be introduced into a wider network, to take into account for the physical constraints given by what that lies upstream and downstream of the considered section, as detailed in the following section.

2.3. Circuital analysis

The information contained in $[\boldsymbol{M}]$ has been derived via a series of "classic" 2D-FEM simulations. This means that the currents obtained through (6) pertain to infinite conductors, whose return path is not physically consistent. In other words,

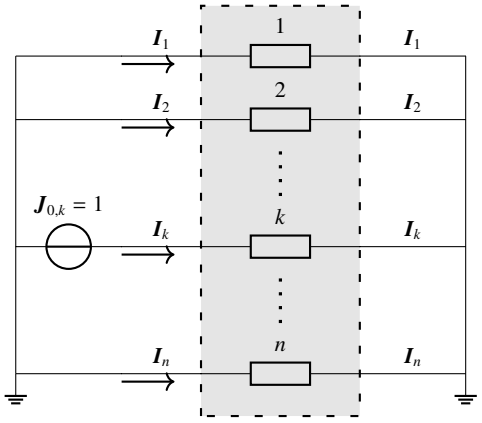

Figure 2: Scheme of the characteristic matrix extraction through the FEM analysis.

there is no guarantee that the sum of the computed axial currents $\boldsymbol{I}_1, \boldsymbol{I}_2, \ldots, \boldsymbol{I}_n$ will be null as it is supposed to be. Therefore, the requirement of a balanced set of currents implies the imposition of some sort of constraint on the forcing terms $\{\boldsymbol{J}_{z,0}\}$ appearing in (6). This is physically equivalent to force those currents through a consistent closed path. Moreover, the various ways for a conductor to be grounded should be representable. This includes non-ideal earthings, coatings etc. Finally, the presence of power sources and loads has to be considered. In order to accomplish this task, as anticipated in Sec. 2.2, the result of the 2D-FEM simulations is used in the framework of a circuital analysis, building a network that includes the multi-port component discussed in the previous section, and described by the constitutive law (6). This network is formed by a total number of branches $n_t = n+n_a$, in which n is the rank of the employed characteristic matrix, and n_a the number of branches added in order to complete the network. The *Tableau Analysis* [13] can be very helpful in accomplishing this task. This technique allows finding any branch voltage $\boldsymbol{V}$, branch current $\boldsymbol{I}$ or node potential $\boldsymbol{e}$ of any network once the information about the topology, the branch equations and the forcing terms is provided. This is performed by writing and solving a linear system of the kind herein

defined:

$$\underbrace{\begin{bmatrix} Id & 0 & -A^T \\ 0 & A & 0 \\ \alpha & \beta & 0 \end{bmatrix}}_{\boldsymbol{T}} \underbrace{\begin{Bmatrix} \boldsymbol{V} \\ \boldsymbol{I} \\ \boldsymbol{e} \end{Bmatrix}}_{\boldsymbol{x}} = \underbrace{\begin{Bmatrix} 0 \\ 0 \\ \boldsymbol{u}_f \end{Bmatrix}}_{\boldsymbol{rhs}}. \tag{9}$$

Looking at (9), $[A]$ is the reduced incidence matrix for the given topology and $[Id]$ the identity matrix. The two matrices $[\alpha]$ and $[\beta]$ contain the coefficients of the branch equations, and the array $\left\{\boldsymbol{u}_f\right\}$ the forcing terms. Equation (9) gathers three sets of equations:

- $[Id]\{\boldsymbol{V}\} - [A^T]\{\boldsymbol{e}\} = 0$, Kirchhoff's Voltage Law (KVL);
- $[A]\{\boldsymbol{I}\} = 0$, Kirchhoff's Current Law (KCL);
- $[\alpha]\{\boldsymbol{V}\} + [\beta]\{\boldsymbol{I}\} = \left\{\boldsymbol{u}_f\right\}$, branch equations.

Once $\boldsymbol{T}$ has been obtained, the unknown array can be computed as:

$$\{\boldsymbol{x}\} = [\boldsymbol{T}]^{-1}\{\boldsymbol{rhs}\}. \tag{10}$$

In order to be included in the Tableau Analysis formulation, the Kirchhoff's Voltage Law (KVL) and branch equations in (9) have to be re-written with the variables used in the FEM code. To do so, the generic branch voltage $\boldsymbol{V}$ has to be related with $\boldsymbol{J}_{0,z}$. This can be done recalling that $\boldsymbol{J}_{0,z} = \sigma \boldsymbol{E}_{0,z}$ and that $\boldsymbol{E}_{0,z} = \boldsymbol{V}/L$, where L is the length of the considered parallel exposure. For a network comprising $n_t = n + n_a$ branches, the KVL can be rewritten as:

$$[R]\{\boldsymbol{V'}\} - [A]^T\{\boldsymbol{e}\} = 0, \tag{11}$$

where the array $\{\boldsymbol{V'}\}$ contains the unknown current densities $\boldsymbol{J}_{0,1}, \boldsymbol{J}_{0,2}, \ldots, \boldsymbol{J}_{0,n}$ for the n branches belonging to the $n-$ port, and the unknown voltages for the remaining n_a added branches $V_{n+1}, V_{n+2}, \ldots, V_{n_t}$. $[R]$ is a diagonal conversion matrix, whose $r_{i,i}-$th element is equal to $\rho_i L$ for the n branches $\in [\boldsymbol{M}]$, and $r_{i,i} = 1$

otherwise:

$$[R] = \begin{bmatrix} \rho_1 L & & & & \\ & \ddots & & \mathbf{0} & \\ & & \rho_n L & & \\ & & & 1 & \\ & \mathbf{0} & & & \ddots \\ & & & & 1 \end{bmatrix}. \tag{12}$$

Any forcing term (that could be the case for the phase conductors when the load flow data are available) have to be included in the array $\left\{\boldsymbol{u}_f\right\}$, pertaining to the right-hand side of the linear system. As anticipated, the branch equations have to be expressed using the variables of the FEM analysis. Hence the relation bounding the currents and voltages of the network becomes:

$$[\alpha]\left\{\boldsymbol{J}'_{0,z}\right\} + [\beta]\left\{\boldsymbol{I}'\right\} = \left\{\boldsymbol{u}_f\right\}, \tag{13}$$

in which the two matrices $[\alpha]$ and $[\beta]$ are obtained by assembling $\alpha_{i,j} \in [\alpha]$ and $\beta_{i,j} \in [\beta]$ for every branch of the network (defined by the nodes i and j). If the $i, j-$th branch belongs to $[\boldsymbol{M}]$ its constitutive relation is expressed by (6), and therefore $\alpha_{i,j} = -m_{h,k}$, where $m_{h,k} \in [\boldsymbol{M}]$, $\beta_{i,j} = 1$ and the corresponding value of u_f is set to zero. Instead, if the $i, j-$th branch represents any other circuital element, i.e., a current generator, an impedance etc., $\alpha_{i,j}$ and $\beta_{i,j}$ have to match the constitutive relation of the given electrical component. As an example, for an impedance $\boldsymbol{Z}_{i,j} = 5\Omega$, $\alpha_{i,j} = 1$, $\beta_{i,j} = -5$ and $u_f = 0$, whereas for a current generator $Ig_{i,j} = 10\ A$ $\alpha_{i,j} = 0, \beta_{i,j} = 1$ and $u_f = 10$. Summarizing, (9) has been rewritten in order to incorporate the variables of the finite element analysis, and finally takes the following form:

$$\underbrace{\begin{bmatrix} \rho L & 0 & -A^T \\ 0 & A & 0 \\ \alpha & Id & 0 \end{bmatrix}}_{\boldsymbol{T}} \underbrace{\begin{Bmatrix} \boldsymbol{J}'_{z,0} \\ \boldsymbol{I}' \\ \boldsymbol{e} \end{Bmatrix}}_{\boldsymbol{x}} = \underbrace{\begin{Bmatrix} 0 \\ 0 \\ \boldsymbol{u}_f \end{Bmatrix}}_{\boldsymbol{rhs}}. \tag{14}$$

Once the linear system has been solved, the currents and voltages are known for each branch of the equivalent network. However, the solution of (14) also yields

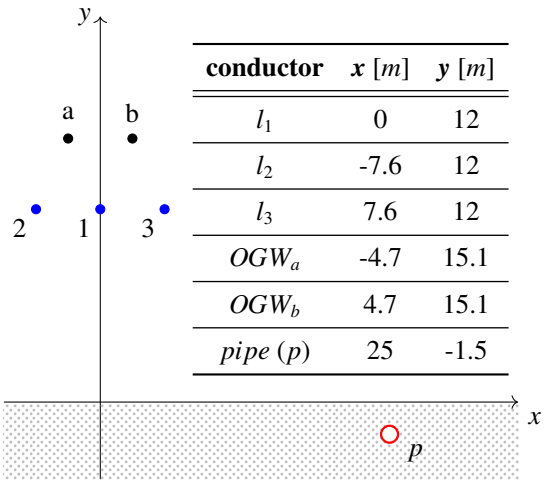

conductor	x [m]	y [m]
l_1	0	12
l_2	-7.6	12
l_3	7.6	12
OGW_a	-4.7	15.1
OGW_b	4.7	15.1
pipe (p)	25	-1.5

Figure 3: Scheme of the configuration (section) for Test I: three-phase overhead power line (blue) with a buried pipeline (red). One and two OGWs (black) are added for Test II and III respectively.

the value of $\boldsymbol{J}_{z,0}$ for the branches belonging to the characteristic matrix. This means that the obtained set of $\boldsymbol{J}_{z,0}$ can be used as the input of a FEM simulation, allowing to compute the distribution of the electromagnetic fields in the calculation domain generated by the currents and voltages computed with (14).

3. Results and discussion

In order to perform a validation of the proposed methodology, a standard case of a parallel exposure of a buried pipeline and an overhead power line is considered in Sec. 3.1. The induced current on the pipeline is computed using both the quasi-3D approach presented in this paper and the methodology proposed by Cigré in [1]. As an example of the possibilities offered by the quasi-3D method, Sec. 3.2 takes into account a more complex case involving 2 OGWs. The induced current on the pipeline is evaluated as the horizontal distance of the pipeline (with respect to the central line conductor of the power line) ranges from 0 to 100 m. In Sec. 3.3, the effects of two non-homogeneous soil resistivity distributions on the computed pipeline current have been assessed.

3.1. Numerical validation

The analytic methodology proposed by Cigré in the well known technical standard [1] is often used as a reference term for new calculation methods [14], and hence will be employed for the validation process of this work. This methodology relies on the classic Carson's formulae for the calculation of the self and mutual impedances of the earth-return circuits under analysis (in our case, the OGW and the pipeline). Any mathematical detail regarding the implementation and subsequent use of these formulae can be found in [10], whereas the information regarding the geometrical disposition of the conductors and their electrical characteristics is summarized in Fig. 3 and Tab. 1, respectively. Actually, three tests (I, II and III) are carried out: for Test I only the power line and the buried pipeline are considered, whereas in Test II the OGW (a) is added. Finally, Test III includes both OGWs (a) and (b). The computations are performed assuming a length of the exposure of $L = 1$ km, and the pipeline is supposed to be earthed at both endings, with a resistance $R_{pipe-s} = 10\ \Omega$. Moreover, as reported in Tab. 1, the pipeline is considered coated by an insulating layer, whose per-unit-length admittance $y' = 1.57 \cdot 10^{-4} + j5.46 \cdot 10^{-6}$ S/m is obtained with the following expression [1]:

$$y' = \frac{\pi D}{\rho_c \delta_c} + j\omega \frac{\epsilon_0 \epsilon_r \pi D}{\delta_c}, \tag{15}$$

in which D is the diameter of the pipeline, ϵ_0 the electric permittivity of the vacuum, $\epsilon_{r_{coat}}$ the relative permittivity of the pipeline's coating, δ_{coat} and ρ_{coat} its thickness and resistivity, respectively. For the three tests, a balanced three phase system of currents $\boldsymbol{I}_1 = 778\underline{/0°}$, $\boldsymbol{I}_2 = 778\underline{/-120°}$, $\boldsymbol{I}_3 = 778\underline{/-240°}$ A is enforced on the line conductors l_1, l_2, l_3 of the power line respectively. Regarding the proposed quasi-3D approach, the characteristic matrix $[\boldsymbol{M}]$ is extracted (following the procedure described in Sec. 2.2) from a mesh consisting of 66121 nodes and 132080 triangular elements, representing the described geometry. The mesh has a circular shape, the top half representing the air surrounding the power line, and the bottom half being the soil.The dimensions of the domain were chosen in such

Table 1: Geometrical and electrical data

$radius - OGW$	5.75	$[mm]$
$radius(ext) - pipe$	0.25	$[m]$
$radius(int) - pipe$	0.23	$[m]$
$\sigma - soil$	$2 \cdot 10^{-2}$	$[S/m]$
$\sigma - OGW$	$5.9 \cdot 10^{7}$	$[S/m]$
$\sigma - pipe$	$5 \cdot 10^{6}$	$[S/m]$
$\mu_r - pipe$	$1.8 \cdot 10^{3}$	$[-]$
$\delta_{coat} - pipe$	4	$[mm]$
$\rho_{coat} - pipe$	$2.5 \cdot 10^{6}$	$[\Omega \cdot m]$
$\epsilon_{r_{coat}} - pipe$	5	$[-]$

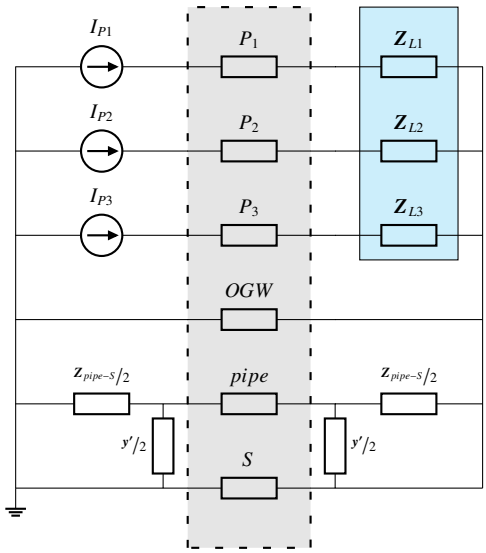

Figure 4: Equivalent electrical circuit for Test II: power line, perfectly earthed OGW, pipeline with imperfect coating and earthing.

Table 2: Validation results

Computed Current	Test I	Test II	Test III
$\boldsymbol{I}_{OGW\ a}$ Cigré	–	87.35/95.34°	87.35/95.34°
$\boldsymbol{I}_{OGW\ a}$ Quasi 3D	–	64.85/1.26°	91.93/1.18°
$\boldsymbol{I}_{OGW\ b}$ Cigré	–	–	87.32/−1.16°
$\boldsymbol{I}_{OGW\ b}$ Quasi 3D	–	–	98.37/−78.87°
$\boldsymbol{I}_{pipe}$ Cigré	2.69/−2.27°	4.93/−7.64°	3.3/18.67°
$\boldsymbol{I}_{pipe}$ Quasi 3D	2.67/−2.25°	4.13/−2.18°	2.69/9.58°
$\Delta\lvert\boldsymbol{I}\rvert_{pipe}$	0.74 %	16.23 %	18.48 %

a way that its extension was greater than the skin depth at the given network frequency. An additional convergence analysis has been performed to ensure that an increase of the domain dimensions leads to negligible variations in the computed results. As a result, considering a non magnetic soil with a $2\,10^{-2}$ S/m conductivity (that is, a 511 m skin depth at a frequency of 50 Hz), the radius length of the semicircles representing the soil and the overlying air region was set to 600 m. A Dirichlet boundary condition was enforced on the value of the magnetic vector potential on the edge of the domain, by setting $\boldsymbol{A}_z = 0$. Concerning the circuital part of the method, an equivalent network is computed by merging the information contained in $[\boldsymbol{M}]$, the value of admittance to earth y' and the pipeline-to-soil grounding resistance R_{pipe-S}. A graphical representation of the circuit is provided in Fig. 4 for Test II, when a single OGW is considered. It should be noticed that in this case the power line three phase load has been added for the sake of completeness, but it does not affect the phase currents, as these have been enforced. The computed current on the pipeline $\boldsymbol{I}_{pipe}$ using both the classic Cigré method and proposed FEM based approach can be found in Tab. 2. As one can see, the two approaches yield a similar trend in the computed pipeline current when the OGWs are added, i.e., both methods show an increase in the induced current magnitude when one OGW is included, and a subsequent decrease when a second one is added. However, the agreement between the two approaches is very good for the configuration without the OGWs, but it rapidly worsen when OGWs are present.

Indeed, as already discussed in [10], any approach based on Carson's formulae relies on the so-called weak coupling hypothesis [15], which is implemented so that the currents of the power line are able to induce electromotive forces on the OGWs and on the pipeline, but the currents on the OGWs and the pipeline do not produce any effect on the power line. Similarly, a current flowing through an OGW is able to produce electromagnetic effects on the pipeline, but not vice versa. Finally, all the mutual interactions between two or more OGWs are ignored, as well as any effect produced by the currents flowing through the soil on every other conductor. This can easily be observed by comparing Tests II and III in Tab. 1: the value of $\boldsymbol{I}_{OGW\ a}$ obtained with the Cigrè method in Test II is retained in Test III even if a second OGW (b) is added. Besides, the amplitude of $\boldsymbol{I}_{OGW\ b}$ is the same of OGW a, in spite of the pipeline being closer to OGW b. On the other hand, this unphysical behaviour is not present in the results of the quasi-3D approach, where all the mutual influences between the conductors are taken into account. As a matter of fact, the above assumptions imply any analytical method based on Carson's formulae introduces considerably stronger approximations when one or more OGWs are present. This fact has been analysed theoretically and numerically in [10]. The above discussion may be used to explain the results reported in the last row of Tab. 2, where $\Delta|I|$ represents the percent difference between the currents obtained with the two approaches, with $\Delta|I| = (\boldsymbol{I}_{pipe}\ \text{Cigré} - \boldsymbol{I}_{pipe}\ \text{quasi 3D})/\boldsymbol{I}_{pipe}\ \text{Cigré} \cdot 100$. As can be observed, $\Delta|I|$ sharply increases when a single OGW is taken into account. The further increase in $\Delta|I|$ obtained when two OGWs are considered is due to the neglecting the mutual interaction between the OGWs adopted in the Cigré approach.

3.2. Induced current evaluation for a pipeline displacement

In order to show some of the possibilities provided by this quasi-3D approach, let's see how the described methodology applies to performing parametric simulations. In particular, given a specific power line configuration, one may be interested to know how the induced current on the pipeline changes with its distance from the power line. In order to accomplish this task, defining d as the horizon-

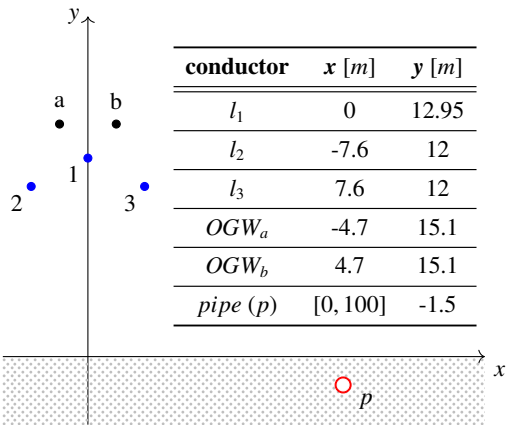

conductor	x $[m]$	y $[m]$
l_1	0	12.95
l_2	-7.6	12
l_3	7.6	12
OGW_a	-4.7	15.1
OGW_b	4.7	15.1
pipe (p)	$[0, 100]$	-1.5

Figure 5: Test configuration: three-phase overhead power line with two overhead ground wires (OGW) and a buried pipeline (section).

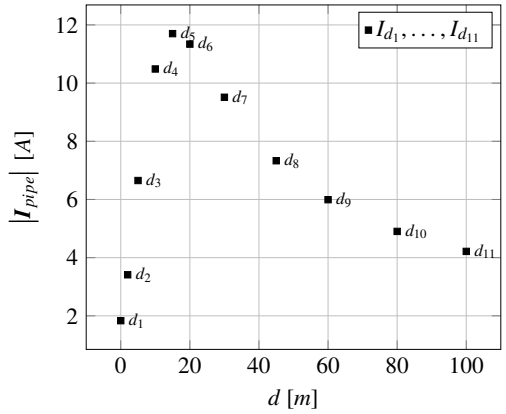

Figure 6: Computed values of $|\boldsymbol{I}_{pipe}|$ horizontal distances of the pipeline $d_1, d_2, \ldots, d_{11}$.

tal distance of the pipeline from the conductor l_1 of the power line, we consider 11 different meshes (with the same characteristics of the one described in Sec. 3.1), corresponding to 11 values of d (i.e., $d_1, d_2, \ldots, d_{11}$). The power line and OGW configuration (which has been retained for all of the 11 displacements) is depicted in Fig. 5. The 11 obtained characteristic matrices $[\boldsymbol{M}]_1, [\boldsymbol{M}]_2, \ldots, [\boldsymbol{M}]_{11}$ have been used to build a corresponding number of electrical circuits, each one consisting of a three phase power line with 2 perfectly earthed OGWs and a perfectly coated pipeline, earthed at both ends with $R_{pipe-s} = 1\Omega$. For each one of these, the values of the currents flowing through all the branches have been

Table 3: Computed currents for Fig. 6

$d\ [m]$	$\boldsymbol{I}_{pipe}\ [A]$
$d_1 = 0$	$1.83\angle 77.88°$
$d_2 = 2$	$3.41\angle 32.83°$
$d_3 = 5$	$6.65\angle 20.26°$
$d_4 = 10$	$10.5\angle 18.35°$
$d_5 = 15$	$11.7\angle 18.80°$
$d_6 = 20$	$11.3\angle 19.25°$
$d_7 = 30$	$9.51\angle 20.05°$
$d_8 = 45$	$7.33\angle 21.21°$
$d_9 = 60$	$5.99\angle 22.11°$
$d_{10} = 80$	$4.90\angle 22.80°$
$d_{11} = 100$	$4.22\angle 22.98°$

computed using the Tableau Analysis described in Sec. 2.3, assuming length of the exposure of 1 *km*. The amplitude of the computed pipeline current versus the horizontal distance d is plotted in Fig. 6 and detailed in Tab. 3. Interestingly, the minimum value of induced current happens to be exactly under the power line, and a local maximum can be seen for a horizontal distance of about 15 m. Now, if the value of the induced current has to be computed at a distance not corresponding to any mesh, the $m_{i,j}(d)$ element of the $[\boldsymbol{M}(d)]$ current matrix relative to any distance $d \in [d_1, d_{11}]$ can be obtained through an interpolation of the $m_{i,j}(d_1, d_2, \ldots, d_{11})$ elements of the $[\boldsymbol{M}]_1, [\boldsymbol{M}]_2, \ldots, [\boldsymbol{M}]_{11}$ sampled characteristic matrices. Figure 7 shows the computed pipeline current when 201 characteristic matrices, obtained from an interpolation of the 11 "sampled" ones, are employed. In order to check the accuracy of this approach, three further dedicated set of FEM calculations have been carried out to evaluate the characteristic matrices $[\boldsymbol{M}(7.5)]$, $[\boldsymbol{M}(25)]$ and $[\boldsymbol{M}(70)]$, respectively corresponding to the three distances $d = 7.5,\ d = 25,\ d = 70$ m. The subsequently obtained values of $\boldsymbol{I}_{pipe}$ are used for a comparison with the ones yielded by the interpolation in Tab. 4. Likewise, the

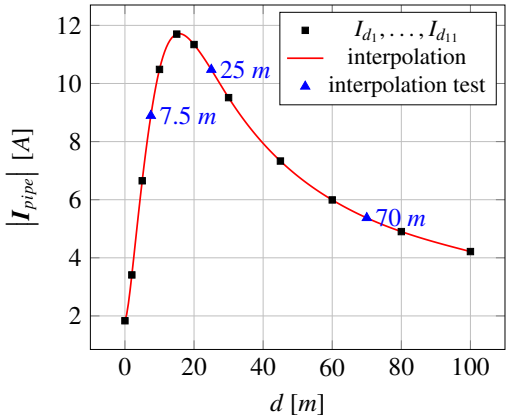

Figure 7: $|\boldsymbol{I}_{pipe}|$ obtained for the configuration of Fig. 5 from the interpolation of the 11 characteristic matrices corresponding to $d_1, d_2, \ldots, d_{11}$.

Table 4: Interpolation test

d [m]	$\boldsymbol{I}_{pipe}$ [A] - reference	$\boldsymbol{I}_{pipe}$ [A] - interpolated
7.5	$8.832\angle 18.50°$	$8.830\angle 18.49°$
25	$10.58\angle 19.66°$	$10.61\angle 19.67°$
70	$5.373\angle 22.53°$	$5.372\angle 22.53°$

geometry described in Fig. 8 has been analysed in order to assess the profile of the induced currents when an asymmetric configuration of the power line is employed. Given the described geometrical disposition of the conductors, it is worth computing the induced current on the pipeline for both positive and negative horizontal distances of the pipeline itself. As Fig. 9 shows, in such cases placing the pipeline at the left (or, dually, at the right) of the power line grants a substantial lowering of the induced currents. As anticipated, the great compatibility of the results shows that just a few number of "sampled" meshes can provide reliable results for a wide range of positions of the considered conductors, thus granting great flexibility to the proposed methodology. Further data regarding the influence of the geometrical disposition of the power line conductors on the induced current levels on the pipeline can be found in [16]. Finally, in order to provide an example of what was stated in Sec. 2.3, the set of $\boldsymbol{J}_{0,z}$ computed using the Tableau Analysis for the configuration depicted in Fig. 5 for $d = 15$ m is used as an input for a 2D-

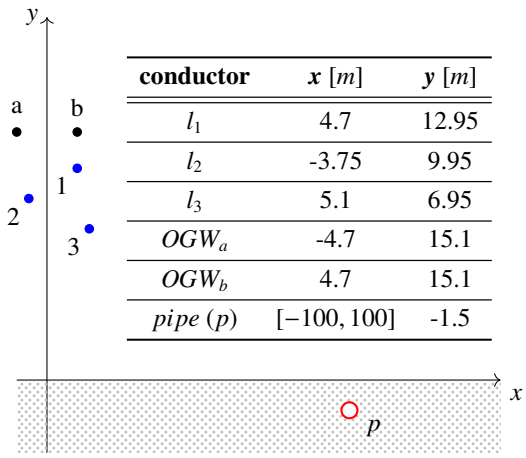

conductor	x [m]	y [m]
l_1	4.7	12.95
l_2	-3.75	9.95
l_3	5.1	6.95
OGW_a	-4.7	15.1
OGW_b	4.7	15.1
$pipe$ (p)	$[-100, 100]$	-1.5

Figure 8: Test configuration: asymmetric three-phase overhead power line with two overhead ground wires (OGW) and a buried pipeline (section).

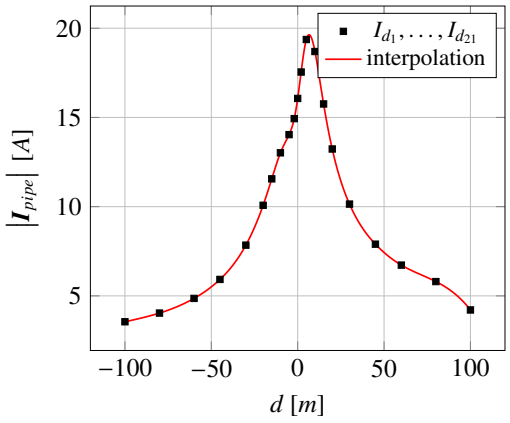

Figure 9: $|\boldsymbol{I}_{pipe}|$ induced by the asymmetric power line configuration of Fig. 8 $d \in [-100, 100]$ [m].

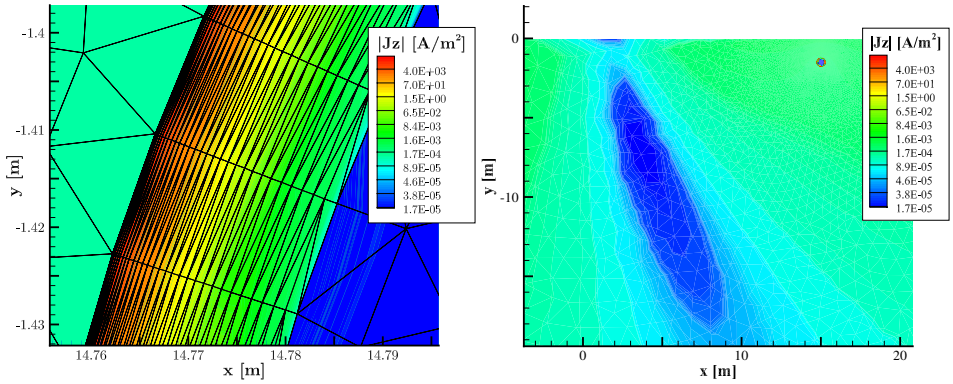

(a) (b)

Figure 10: $|\boldsymbol{J}_{z,0}|$ distribution over the pipeline section (a) and below the power line (b) for the geometry of Fig. 5 with $d = 15$ $[m]$. The pipeline is shown in the top-right corner of (b).

FEM simulation, which consequently yields the electromagnetic field distribution corresponding to the computed set of branch voltages and currents. A detail of the obtained current density distribution on a portion of the pipeline and in the soil below the power line is shown in Fig. 10 (a) and (b) respectively.

3.3. Complex soil analysis

Up to this point, all the provided examples shared the assumption of a homogeneous soil, for the sake of simplicity. However, one of the great advantages of FEM-based techniques is the ability to reproduce soil configurations of any complexity level. In order to provide a demonstration of such capabilities, two non-homogeneous soil configurations are here presented. In the first proposed case study, the soil has been modelled with three horizontal layers with different electrical conductivities, whereas in the second the electrical conductivity of the soil is described by an analytical function, aiming to obtain an unsymmetrical stratified structure. To the authors' knowledge, while multi-layered soil models have already been developed [4] for horizontal and vertical layers, a non-symmetrical and continuous soil resistivity is by no means representable in the framework of a Carson's formulae based approach.

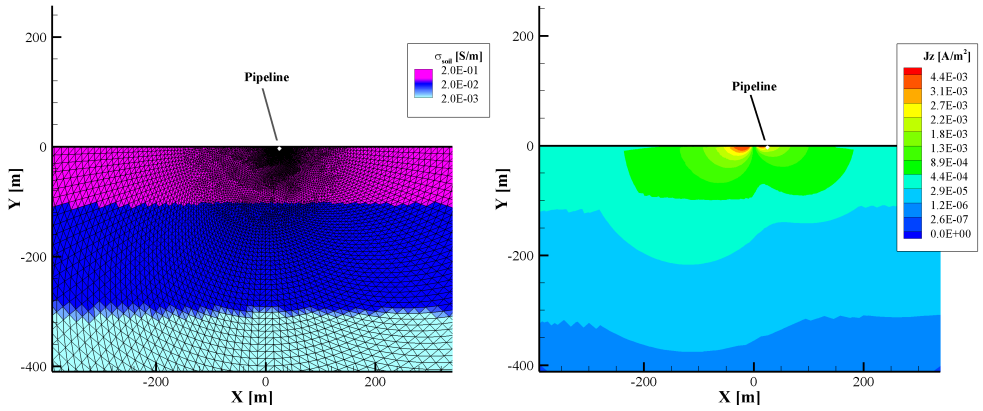

(a) (b)

Figure 11: Three-layer electrical conductivity of the soil (a) and the corresponding obtained current density distribution (b).

3.3.1. Three-layered soil conductivity

As anticipated, the first presented test case aims to show how the current density distribution in the soil (and hence in the pipeline) can be altered by a non-uniform soil structure. In order to do so, the electrical and geometrical configuration described in Fig. 3 and Tab. 1 has been employed, with the soil structure being the only changed parameter. Figure 11 shows the three adopted layers: starting from the ground level, the upper layer has a conductivity σ_1 of 0.2 S/m and a thickness of 100 m. The second and the third layers are 200 m and 300 m thick, and their electrical conductivities have been set to $\sigma_2 = 0.02$ S/m and $\sigma_3 = 0.002$ S/m respectively. The described soil conductivity distribution is shown in Fig. 11 (a). Figure 11 (b) illustrates the current density distribution induced in the soil when a balanced set of currents of amplitude 778 A is enforced on the conductors of the power line, and a single OGW is present. As can be seen, the increases in the soil resistivity are followed by a corresponding decrease in the induced current density profile. The asymmetric profile of the current density distribution is due to both the presence of a single OGW and the screening effect of the pipeline, located 25 m right with respect to the power line.

The first row of Tab. 5 shows I_{unif}, that is, the obtained pipeline current inten-

Table 5: Uniform and multi-layered soil comparison

σ_1	σ_2	σ_3	$\boldsymbol{I}_{pipe}$ $[A]$	$\Delta\|I\|$
$2 \cdot 10^{-2}$	$2 \cdot 10^{-2}$	$2 \cdot 10^{-2}$	$4.13\angle{-2.18°}$	-
$2 \cdot 10^{-1}$	$2 \cdot 10^{-2}$	$2 \cdot 10^{-3}$	$3.80\angle{0.89°}$	-7.99%
$2 \cdot 10^{-2}$	$2 \cdot 10^{-2}$	$2 \cdot 10^{-3}$	$4.33\angle{-2.82°}$	4.84%
$2 \cdot 10^{-3}$	$2 \cdot 10^{-2}$	$2 \cdot 10^{-3}$	$4.64\angle{-4.54°}$	12.59%

sity using a uniform soil and the configuration of Sec 3.1 with the single OGW (a). This result, taken a reference, is compared against the ones obtained by employing the described three-layer soil structure. The last column on of the table shows $\Delta|I|$, i.e., the percent difference between the given computed pipeline current amplitude I and the reference current I_{unif}, defined as $\Delta|I| = (I - I_{unif})/I_{unif} \cdot 100$. The different obtained values of $\Delta|I|$ show the relevance of the soil structure in determining the current induced on the pipeline. Finally, it should be noticed that the obtained behaviour of the induced current agrees with both theoretical and practical existing results [1], indicating that higher electromagnetic induction levels on the pipeline are expected, when the soil electrical resistivity increases.

3.3.2. Analitically defined soil conductivity

This second test case shares with the previous one all the geometrical and electrical parameters, except for the electrical conductivity of the soil. In particular, the electrical conductivity is described by a continuous, analitically defined, function of the coordinates x and y:

$$\sigma_{soil} = \sigma_2 + \sigma_1 \, exp\left(-\left(\frac{y}{20}\right)^2\right) + \sigma_3 \, exp\left(-\left(\frac{y - y_{cnt}}{10}\right)^2\right), \tag{16}$$

with,

$$y_{cnt} = -70 + 10 \, \tan^{-1}\left(\frac{x - 15}{10}\right). \tag{17}$$

The three parameters σ_1, σ_2 and σ_3 have been set to 0.2, 0.02 and 0.002 S/m respectively. As shown in Fig. 12 (a), the employment of a Gaussian-like distributed electrical conductivity allowed obtaining a smooth transition between different

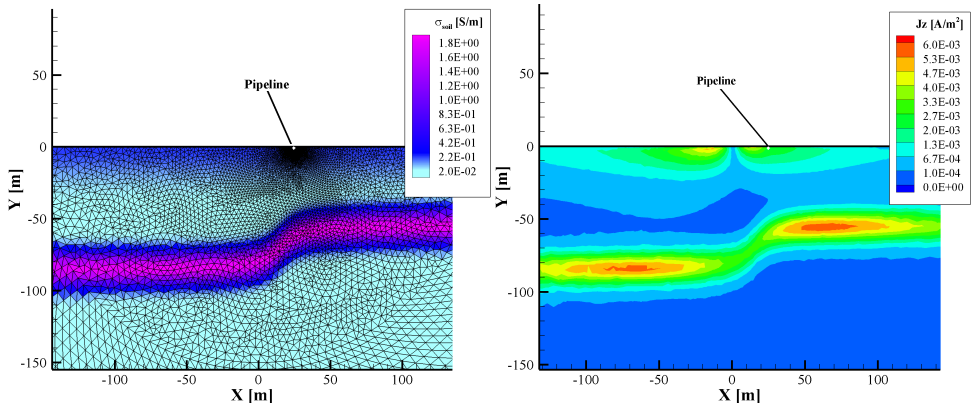

(a) (b)

Figure 12: Analytically-defined electrical conductivity of the soil (a) and the corresponding obtained current density distribution (b).

soil layers, that do not have to be either horizontal or vertical as in the classic analytical models. As expected, the computed current density is clearly affected by the soil structure, as highlighted in Fig. 12 (b). The obtained pipeline current for this configuration is $3.65\angle 2.08°$ A. This result can be compared with the $4.13\angle 2.18°$ A, obtained for a homogeneous soil with a conductivity of 0.02 S/m, to emphasize how heavily the soil structure can affect the induced current on the pipeline.

4. Conclusion

A quasi-3D method for the analysis of the interference induced on a buried pipeline by an overhead power line is presented in this paper. The method is based on a 2D-FEM analysis carried out on a section of a corridor, coupled with an electric network to account for the third dimension. This approach presents two main advantages over the classic circuital methods. Firstly, the FEM analysis offers a deeper insight of the considered problem, yielding the distribution of the electromagnetic fields on the geometry under analysis. Secondly the multi-port component, obtained from the FEM analysis to represent a generic corridor section, embodies the mutual interaction between the conductors (including the soil)

in the given section. The multi-port component, introduced into an electric network, allows one to account for the physical effects produced by what is upstream and downstream of the section, such as imperfect coatings and groundings of the pipeline. Differently from any circuital method based on Carson's formulae or their approximation, the accuracy of the presented approach is not affected by the number and kind of considered conductors. A numerical validation has been performed through the simulation of a 1 km parallel exposure of an overhead power line and a metallic pipeline buried in the soil, characterized by an imperfect coating and earthed at both endings with a non-zero resistance. The comparison with the Cigré standard for this simple case shows that the proposed approach yields consistent and reliable results. A parametric study has been performed by computing the induced current on a buried pipeline for a range of 11 horizontal distances from the power line. It is shown that the characteristic matrices obtained for these geometrical configurations can be conveniently interpolated obtaining reliable results even for geometries that have not been analysed by FEM. Morover, the effects of two non-homogeneous soil resistivity distributions on the computed pipeline current have been computed and discussed to demonstrate the flexibility of the method. It should also be highlighted that the approach here described was developed to assess AC interference problems on pipelines, but is nevertheless totally general. In fact, the approach can be used without any modification to calculate the currents and voltages on any set of long conductors running parallel one to each other, in presence of the soil.

References

[1] CIGRE, Guide on the Influence of High Voltage AC Power Systems on Metallic Pipelines, Technical Report, Cigré Working Group 36.02, 1995.

[2] H. J. Haubrich, B. A. Flechner, W. Machczynski, A universal model for the computation of the electromagnetic interference on earth return circuits, IEEE Transactions on Power Delivery 9 (1994) 1593–1599.

[3] X. Wu, H. Zhang, G. G. Karady, Transient analysis of inductive induced voltage between power line and nearby pipeline, International Journal of Electrical Power & Energy Systems 84 (2017) 47 – 54.

[4] M. Nakagawa, A. Ametani, K. Iwamoto, Further studies on wave propagation in overhead lines with earth return: impedance of stratified earth, in: Proceedings of the Institution of Electrical Engineers, volume 120, number 12, IET, pp. 1521–1528, 1973.

[5] A. Taflove, J. Dabkowski, Prediction Method for Buried Pipeline Voltages Due to 60 Hz AC Inductive Coupling Part I-Analysis, IEEE Transactions on Power Apparatus and Systems PAS-98 (1979) 780–787.

[6] J. Dabkowski, A. Taflove, Prediction Method for Buried Pipeline Voltages Due to 60 Hz AC Inductive Coupling Part II–Field test Verification, IEEE Transactions on Power Apparatus and Systems PAS-98 (1979) 788–794.

[7] G. C. Christoforidis, D. P. Labridis, P. S. Dokopoulos, A hybrid method for calculating the inductive interference caused by faulted power lines to nearby buried pipelines, IEEE Transactions on Power Delivery 20 (2005) 1465–1473.

[8] M. Ouadah, O. Touhami, R. Ibtiouen, M. Benlamnouar, M. Zergoug, Corrosive effects of the electromagnetic induction caused by the high voltage power lines on buried X70 steel pipelines, International Journal of Electrical Power & Energy Systems 91 (2017) 34 – 41.

[9] A. Popoli, A. Cristofolini, L. Sandrolini, B. T. Abe, A. Jimoh, Assessment of AC interference caused by transmission lines on buried metallic pipelines using F.E.M., in: 2017 International Applied Computational Electromagnetics Society Symposium - Italy (ACES), pp. 1–2, 2017.

[10] A. Cristofolini, A. Popoli, L. Sandrolini, A comparison between Carson's formulae and a 2D FEM approach for the evaluation of AC interference

caused by overhead power lines on buried metallic pipelines, Progress In Electromagnetics Research C 79 (2017) 39–48.

[11] C. W. Steele, Numerical Computation of Electric and Magnetic Fields, Springer US, 2nd edition, 1997.

[12] Intel Math Kernel Library Reference Manual - Fortran (2018) 2488 – 2530.

[13] L. O. Chua, C. A. Desoer, E. S. Kuh, Linear and nonlinear circuits, McGraw-Hill College, 1987.

[14] B. Schoonjans, J. Deconinck, Calculation of HVAC inductive coupling using a generalized BEM for Helmholtz equations in unbounded regions, International Journal of Electrical Power & Energy Systems 84 (2017) 242 – 251.

[15] C. R. Paul, Introduction to electromagnetic compatibility, John Wiley & Sons, 2006.

[16] A. Popoli, L. Sandrolini, A. Cristofolini, Data on the interference induced on a buried pipeline by an overhead power line, Data in Brief (submitted for publication) (2018).